HEFAT2003
2nd International Conference on Heat Transfer, Fluid Mechanics and Thermodynamics
23 – 26 June 2003, Victoria Falls, Zambia
Paper number: GV1

QUASI-3D SIMULATION OF COMPRESSIBLE UNSTEADY FLOWS

Victor Gheorghiu
Department of Mechanical Engineering
University of Applied Sciences Hamburg, Germany
Berliner Tor 21, 20099 Hamburg, Germany
E-mail: grg@rzbt.haw-hamburg.de

ABSTRACT

The purpose of this paper is to present a new computation method of the unsteady compressible flow process of a viscous fluid through pipes and manifolds for example of internal combustion engines (ICE). This method can describe the influence of the gas flow three-dimensionality correctly (i.e. curvatures, asymmetry of the pipes and channels etc.), that improves the simulation quality noticeably (compared to the classical 1D-simulation) without increasing the cost of computation proportionally (compared to the classical 3D-simulation). This method is referred to as the **quasi-3D method** in the following. Apart from some theoretical basics, the quasi-3D method is applied (as an example) to a one-cylinder research diesel engine. The comparison between simulation results in intake pipe and cylinder and pressure measurements in multi-point intake pipe at one engine speed and two loads is shown and commented.

INTRODUCTION

The design of intake and exhaust ICE manifolds has been an important application of unsteady fluid dynamics for many years. A first purpose of these simulations is the optimizing of the cylinder filling, the accordance with the turbocharger etc. about wide load and engine speed intervals. A second purpose is the estimating of the required initial conditions for the simulation of the in cylinder air/fuel mixture formation and burning processes, which must have knowledge about the quantity, the composition and the flow-field of the intake charge.

Since the computation costs are high for the implementation of unsteady three-dimensional (3D) simulations of the gas exchange processes usual one-dimensional (1D) simulations are used instead. In this case, since the 1D-simulation of the gas flow processes cannot describe the whole reality (i.e. the three-dimensionality) of the gas flow correctly, curvatures, asymmetry of the pipes and channels in the simulation are disregarded.

In order to find a compromise procedure for this situation, the **quasi-3D method** is introduced. It is based on the 1D partial differential equations (PDEs), which models the unsteady compressible flow process of a viscous fluid and it is introduced now in the following steps:

1. The 3D flow equations are deduced appropriately, as to consider the distortion of the velocity distribution (size and direction) in each pipe cross-section. Their integration over the pipe cross-section results in the 1D flow equations, the terms of which still contain integrals of the velocity distribution. In the following, these integrals are designated as **adjustment coefficients** of the 1D flow, since they describe the 3D distribution of the gas flow velocity. The 1D flow equations together with the adjustment coefficients form **the quasi-3D PDEs**.
2. The adjustment coefficients are further treated as temporally independent parameters in each pipe cross-section. For integration of the quasi-3D PDEs the total variation diminishing (TVD) finite difference method (as example) is used. The quasi-3D PDEs are processed accordingly here, and the application of the TVD procedure is presented in detail.
3. The determination of the adjustment coefficients, which consider the three-dimensionality of the gas flow, take place with the help of a steady 3D-simulation. Programs such as STAR CD, FIRE, KIVA 3, Flow-3D etc. can be used for this simulation. The 3D-simulation is only done for steady forward and reverse flow through the pipes. The resulted 3D flow velocity fields are appropriately processed to produce the requested adjustment coefficients.
4. The quasi-3D method can be used now for the accurate simulation of manifold flow processes throughout the full engine cycles.

DERIVATION OF THE QUASI-3D PDES

For the theoretical development of the 1D PDEs it is helpful to use the stream thread notion. In this case the lateral surface of the stream thread is impermeable to matter, since this area itself is formed by streamlines. The classical stream thread notion is generally characterized as follows: *The variations of all state variables in the cross direction of a stream thread are much lower than in its longitudinal direction* [**13**]. The **quasi-3D stream thread notion** supplements the classical one by accepting that the *flow velocity varies significant in the cross direction too.*

In case of a pipe flow, since the tube wall (similar to the stream thread lateral surface) is impermeable to matter, the quasi-3D stream thread notion can be put into practice perfectly. This notion has the advantage that one can take into account the effect of the interior curvatures, asymmetry etc.

of the pipes and channels on the resulting distorted velocity field.

Continuity equation

The continuity equation for a fluid element with the density ρ is [**4**]

$$(\rho \cdot A)_t + (\rho \cdot C \cdot A)_x = 0 \,. \tag{1}$$

in which the subscripts t and x denotes partial differentiating with respect to time and to space, and

$$C = \frac{1}{A} \cdot \int_{A(t)} c \cdot dA \,. \tag{2}$$

is the average value of the local axial flow velocity c over the stream thread cross-section A.

Momentum equation along the stream thread axis

The momentum variation of the fluid element is caused by the mass forces (here negligible) and surface forces. This vectorial equation is now projected upon the stream thread axis and consequently becomes [**4**]

$$(\rho \cdot C \cdot A)_t + \left(\beta \cdot \rho \cdot C^2 \cdot A + p \cdot A\right)_x = p \cdot A_x - \frac{\lambda_D}{D_H} \cdot \frac{\rho \cdot C \cdot |C|}{2} \cdot A \tag{3}$$

in which λ_D is the wall friction coefficient, p the pressure, D_H the hydraulic diameter of the pipe and

$$\beta = \frac{1}{C^2 \cdot A} \cdot \int_{A(t)} c^2 \cdot dA \tag{4}$$

the well-known *Coefficient of Boussinesq* β (s. [**2**], [**3**]).

Energy equation

Here one must note that the specific kinetic energy of the fluid element refers to the local flow velocity $\vec{v}$ and not to its axial part c. This equation processed for an ideal gas becomes [**4**]

$$\left[A \cdot \left(\frac{p}{\kappa - 1} + \gamma \cdot \frac{\rho \cdot C^2}{2}\right)\right]_t + \left[A \cdot C \cdot \left(\frac{\kappa \cdot p}{\kappa - 1} + \alpha \cdot \frac{\rho \cdot C^2}{2}\right)\right]_x = \frac{\lambda_D}{D_H} \cdot \frac{\rho \cdot |C^3|}{2} \cdot A + \frac{4 \cdot k}{D_H} \cdot (T_W - T) \cdot A \,, \tag{5}$$

in which κ means the isentropic exponent, k the heat transfer coefficient, T the gas temperature and T_W the wall temperature. For describing the effect of the flow velocity distribution distortion in the cross-section A the coefficients

$$\gamma = \frac{1}{C^2 \cdot A} \cdot \int_{A(t)} v^2 \cdot dA \,, \tag{6}$$

and

$$\alpha = \frac{1}{C^3 \cdot A} \cdot \int_{A(t)} v^2 \cdot c \cdot dA \tag{7}$$

are introduced. If one wants to insert the axial flow velocity c into equation (5) instead of the local flow velocity $\vec{v}$, i.e. if one wants to assume that the flow velocity is directed only along the stream thread axis, then the coefficients β and γ will have identical calculation formulas. Although their formulas are identical, their physical meanings remain very different. In this case, the coefficient α also becomes simpler and thus identical to the well-known *Coefficient of Coriolis* (s. [**3**], [**5**]).

The coefficients α, β and γ are always greater than one and are designated as **adjustment coefficients** of the 1D flow, since they describe the 3D distortion of the gas flow velocity field in a cross-section A of the stream thread, respectively, of the pipe.

Conservation form of all PDEs

The PDEs represented above can be brought together in a vectorial form as [**4**]

$$\boldsymbol{U}_t + \boldsymbol{F}(\boldsymbol{U})_x = \boldsymbol{H}(\boldsymbol{U}) \,, \tag{8}$$

where

$$\boldsymbol{U} = \begin{bmatrix} \rho \\ \rho \cdot C \\ \dfrac{p}{\kappa - 1} + \gamma \cdot \dfrac{\rho \cdot C^2}{2} \\ r_i \cdot \rho \end{bmatrix} = \begin{bmatrix} U_1 \\ U_2 \\ U_3 \\ U_4 \end{bmatrix} \tag{8.1}$$

$$\boldsymbol{F}(\boldsymbol{U}) = \begin{bmatrix} U_2 \\ (\kappa - 1) \cdot U_3 + \left(\beta - \dfrac{\kappa - 1}{2} \cdot \gamma\right) \cdot \dfrac{U_2^2}{U_1} \\ \dfrac{U_2}{U_1} \cdot \left(\kappa \cdot U_3 + \dfrac{\alpha - \kappa \cdot \gamma}{2} \cdot \dfrac{U_2^2}{U_1}\right) \\ \dfrac{U_2}{U_1} \cdot U_4 \end{bmatrix} \tag{8.2}$$

$$\boldsymbol{H}(\boldsymbol{U}) = \begin{bmatrix} -U_1 \cdot \left(\dfrac{A_t}{A} + \dfrac{U_2}{U_1} \cdot \dfrac{A_x}{A}\right) \\ -U_2 \cdot \left[\left(\dfrac{A_t}{A} + \beta \cdot \dfrac{U_2}{U_1} \cdot \dfrac{A_x}{A}\right) + \dfrac{1}{2} \cdot \dfrac{\lambda_D}{D_H} \cdot \dfrac{|U_2|}{U_1}\right] \\ H_3 \\ -U_4 \cdot \left(\dfrac{A_t}{A} + \dfrac{U_2}{U_1} \cdot \dfrac{A_x}{A}\right) \end{bmatrix} \tag{8.3}$$

with

$$H_3 = \left[-\left(\frac{A_t}{A} + \kappa \cdot \frac{U_2}{U_1} \cdot \frac{A_x}{A}\right) - \frac{4 \cdot k}{D_H} \cdot \frac{\kappa - 1}{U_1 \cdot R_G}\right] \cdot \left(U_3 - \frac{\gamma}{2} \cdot \frac{U_2^2}{U_1}\right) - \frac{1}{2} \cdot \frac{U_2^2}{U_1} \cdot \left[\left(\gamma \cdot \frac{A_t}{A} + \alpha \cdot \frac{U_2}{U_1} \cdot \frac{A_x}{A}\right) - \frac{\lambda_D}{D_H} \cdot \frac{|U_2|}{U_1}\right] + \frac{4 \cdot k}{D_H} \cdot T_W$$

in which R_G is the gas constant.

If all terms in the source terms vector $\boldsymbol{H}$ would be zero, the equation (8) becomes a homogeneous PDE, i.e.

$$\boldsymbol{U}_t + \boldsymbol{F}(\boldsymbol{U})_x = \boldsymbol{0} \,. \tag{9}$$

NUMERICAL INTEGRATION OF QUASI-3D PDES

In this case the finite-difference method with the so-called total variation diminishing (TVD) method, Lax-Friedrichs non-MUSCL (monotonic upstream schemes for conservation laws) approach for the homogeneous PDE (9) is used [**12**]. In order to consider the effect of the source terms from the vector $\boldsymbol{H}$, the TVD technique is integrated in a predictor-corrector procedure [**12**], [**4**].

Processing of the homogeneous PDE

The equation (9) is discretized now with the help of the finite-difference method along the time axis t and the space axis x. Let $\boldsymbol{U}_j^n$ be the numerical approximation of the solution of equation (9) at $x = j \cdot \Delta x$ and $t = n \cdot \Delta t$, with Δx being the spatial mesh size (equally spaced, for simplicity) and Δt the time step. After the application of the finite-difference method in an explicit technique results

$$\boldsymbol{U}_j^{n+1} = \boldsymbol{U}_j^n - \lambda \cdot \left(\boldsymbol{F}_{j+\frac{1}{2}}^n - \boldsymbol{F}_{j-\frac{1}{2}}^n \right), \tag{10}$$

whereas the subscript $j \pm \frac{1}{2}$ points at the middle positions between j and $j \pm 1$. The mesh discretization parameter is

$$\lambda = \frac{\Delta t}{\Delta x}. \tag{11}$$

The vector $\boldsymbol{U}$ at the time $n+1$ here is the unknown quantity. In order to determine it, one must first determine the vector $\boldsymbol{F}$, i.e. the numerical flux, at the positions $j \pm \frac{1}{2}$.

Application of the Lax-Friedrichs non MUSCL scheme

In case of second order schemes, the numerical flux $\boldsymbol{F}$ can be written at the position $j \pm \frac{1}{2}$ utilizing so-called local characteristics [**12**],

$$\boldsymbol{F}_{j+\frac{1}{2}} = \frac{1}{2} \cdot \left(\boldsymbol{F}_j + \boldsymbol{F}_{j+1} + \boldsymbol{R}_{j+\frac{1}{2}} \cdot \boldsymbol{\Phi}_{j+\frac{1}{2}} \right), \tag{12}$$

in which the product $\boldsymbol{R} \cdot \boldsymbol{\Phi}$ is responsible for achieving the second order accuracy. A derivation of the vector $\boldsymbol{\Phi}$ at the position $j + \frac{1}{2}$ can be found in references [**12**] and [**4**].

The right-eigenvector matrix $\boldsymbol{R}$ of the Jacobian matrix

$$\boldsymbol{B}(\boldsymbol{U}) = \frac{d}{d\boldsymbol{U}} \boldsymbol{F}(\boldsymbol{U}), \tag{13}$$

of $\boldsymbol{F}$ is the solution of the equation

$$\boldsymbol{R}^{-1} \cdot \boldsymbol{B} \cdot \boldsymbol{R} = \boldsymbol{\Delta}, \tag{14}$$

where $\boldsymbol{\Delta}$ is the diagonal matrix of the eigenvalues δ_i of $\boldsymbol{B}$

$$\delta_1 = C - a \qquad \delta_2 = C \qquad \delta_3 = C + a \qquad \delta_4 = C. \tag{15}$$

These eigenvalues show the local characteristic directions and form the base e.g. for the application of the *Method of Characteristics*. This method was originally introduced by Riemann [**7**]. It was used, as a graphical technique, by Jenny [**6**] to calculate flows in engine manifolds, and Seifert [**10**] and Benson et al. [**1**] employed it, in the form of the *Mesh Method of Characteristics*.

The adjustment coefficients α, β and γ, which describe the speed distribution distortion in the cross-section A of the stream thread, make the **exact** determination of the eigenvalues of the matrix [**4**]

$$\boldsymbol{B} = \begin{bmatrix} 0 & 1 & 0 & 0 \\ -\left(\beta - \frac{\kappa - 1}{2} \cdot \gamma\right) \cdot C^2 & B_{22} & \kappa - 1 & 0 \\ B_{31} & B_{32} & \kappa \cdot C & 0 \\ -r_i \cdot C & r_i & 0 & C \end{bmatrix}, \tag{16}$$

impossible, where

$$B_{22} = 2 \cdot \left(\beta - \frac{\kappa - 1}{2} \cdot \gamma\right) \cdot C,$$

$$B_{31} = -\frac{a^2 \cdot C}{\kappa - 1} - \left(\alpha - \frac{1}{2} \cdot \kappa \cdot \gamma\right) \cdot C^3,$$

$$B_{32} = \frac{a^2}{\kappa - 1} + \left(\frac{3}{2} \cdot \alpha - \kappa \cdot \gamma\right) \cdot C^2,$$

and a is the local speed of sound of the ideal gas in the stream thread.

Although at present (contrary to the classical 1D case), no exact solution for $\boldsymbol{R}$ from equation (14) is known, one can further reduce the errors introduced for example with the use of $\boldsymbol{R}_{1D}$ (from classical 1D case) instead of $\boldsymbol{R}$ if

$$\boldsymbol{R}_{q3D} = \begin{bmatrix} 1 & 1 & 1 & 1 \\ C - a & C & C + a & C \\ R_{q3D_{31}} & \alpha \cdot \frac{C^2}{2} & R_{q3D_{33}} & \alpha \cdot \frac{C^2}{2} \\ r_i & 0 & r_i & r_i \end{bmatrix} \tag{17}$$

with

$$R_{q3D_{31}} = \frac{a^2}{\kappa - 1} + \alpha \cdot \frac{C^2}{2} - C \cdot a$$

$$R_{q3D_{33}} = \frac{a^2}{\kappa - 1} + \alpha \cdot \frac{C^2}{2} + C \cdot a$$

and its inverse matrix

$$\boldsymbol{R}_{q3D}^{-1} = \begin{bmatrix} R_{q3D_{11}}^{-1} & \frac{-a}{\kappa - 1} - C & 1 & 0 \\ \frac{2 \cdot a^2}{\kappa - 1} & 0 & 0 & \frac{-2 \cdot a^2}{(\kappa - 1) \cdot r_i} \\ R_{q3D_{31}}^{-1} & \frac{a}{\kappa - 1} - C & 1 & 0 \\ -C^2 & 2 \cdot C & -2 & \frac{2 \cdot a^2}{(\kappa - 1) \cdot r_i} \end{bmatrix} \tag{18}$$

with

$$R_{q3D_{11}}^{-1} = \frac{C \cdot a}{\kappa - 1} + (2 - \alpha) \cdot \frac{C^2}{2}$$

$$R_{q3D_{31}}^{-1} = \frac{C \cdot a}{\kappa - 1} + (2 - \alpha) \cdot \frac{C^2}{2}.$$

are used [**4**]. The resulted equation

$$\boldsymbol{R}_{q3D}^{-1} \cdot \boldsymbol{B} \cdot \boldsymbol{R}_{q3D} = \boldsymbol{\Delta}$$

as nearest approximation of the equation (14) can be brought into the form

$$\begin{bmatrix} -a + C - \omega_1 & \omega_1 & \omega_1 & \omega_1 \\ 0 & C & 0 & 0 \\ \omega_2 & \omega_2 & a + C + \omega_2 & \omega_2 \\ \omega_3 & \omega_3 & \omega_3 & C + \omega_3 \end{bmatrix} = \boldsymbol{\Delta} \qquad (19)$$

where

$$\omega = (\kappa - 1) \cdot (1 - \alpha) \qquad \omega_1 = \frac{\omega}{4} \cdot \frac{C^2}{a} \cdot \left(1 - \frac{C}{a}\right)$$

$$\omega_2 = -\frac{\omega}{4} \cdot \frac{C^2}{a} \cdot \left(1 + \frac{C}{a}\right) \qquad \omega_3 = \frac{\omega}{2} \cdot \frac{C^3}{a^2}$$

The following notes are to be made here:

- In the LH member of the equation (19) only the adjustment coefficient α appears as opposed to in equation (14), i.e., β and γ disappear together.
- The equation (19) is valid only, if ω is zero or very small. In fact the magnitude of ω is small because α and κ are close to one.
- The matrices in the equation (19) possess an identical determinant, and this happens independently of the α, ω and κ values.
- The approximation $\boldsymbol{R}_{q3D}$ is closer to the exact matrix $\boldsymbol{R}$ from equation (14) than $\boldsymbol{R}_{1D}$.
- The product $\boldsymbol{R}_{j+\frac{1}{2}} \cdot \boldsymbol{\Phi}_{j+\frac{1}{2}}$ influences equation (12) much less when defining the numerical flux $\boldsymbol{F}_{j+\frac{1}{2}}$ than the sum $\boldsymbol{F}_j + \boldsymbol{F}_{j+1}$, since this product is nearly proportional to the difference $\boldsymbol{F}_j - \boldsymbol{F}_{j+1}$. This fact shows that the errors caused by application of $\boldsymbol{R}_{q3D}$ instead of $\boldsymbol{R}$ in the equation (12), will have a low impact on the accuracy of the scheme.

Roe's averaged state

Independently of using of $\boldsymbol{R}_{1D}$, $\boldsymbol{R}_{q3D}$ or any other form instead of $\boldsymbol{R}$ in equation (12) further means

$$\boldsymbol{R}_{j+\frac{1}{2}} = \boldsymbol{R}\left(\boldsymbol{U}_{j+\frac{1}{2}}\right). \qquad (20)$$

The vector $\boldsymbol{U}_{j+\frac{1}{2}}$ can be defined either roughly as the arithmetic average value between $\boldsymbol{U}_j$ and $\boldsymbol{U}_{j+1}$ or much more accurately with the help of the so-called **average value procedure of Roe** [**8**]. The procedure of Roe supplies the correct average, even if it is applied on different sides of a shock wave or of another discontinuity. Roe's averaged state for the 1D PDE and for a perfect gas for example is discussed in reference [**12**]. In order to determine Roe's averaged state for the quasi 3D-flow model equation (13) is discretized

$$\boldsymbol{F}_{j+\frac{1}{2}} - \boldsymbol{F}_{j-\frac{1}{2}} = \overline{\boldsymbol{B}} \cdot \left(\boldsymbol{U}_{j+\frac{1}{2}} - \boldsymbol{U}_{j-\frac{1}{2}}\right). \qquad (21)$$

The components of the Jacobian matrix $\overline{\boldsymbol{B}}$ are now the averaged values of the state variables. The vectorial equation (21) contains four scalar equations.

The first one is easily fulfilled. In order to be able to process the other three scalar equations, the following positive auxiliary parameter has to be introduced

$$\varepsilon = \sqrt{\frac{\rho_{j+\frac{1}{2}} \cdot A_{j+\frac{1}{2}}}{\rho_{j-\frac{1}{2}} \cdot A_{j-\frac{1}{2}}}}. \qquad (21)$$

Two solutions result for the axial speed from the second scalar equation of (21) at the position $j \pm \frac{1}{2}$

$$C_{j+\frac{1}{2}} = \frac{C_j + \varepsilon \cdot C_{j+1}}{1 + \varepsilon} \qquad (22)$$

$$C_{j+\frac{1}{2}} = \frac{C_j - \varepsilon \cdot C_{j+1}}{1 - \varepsilon}. \qquad (22')$$

From these there is the benefit that (22) have not unsteadiness (because $\varepsilon > 0$) and for this reason further only it is applied.

From the third scalar equation of (21) it results for the averaged value of the specific total enthalpy

$$h_{j+\frac{1}{2}} = \frac{h_j + \varepsilon \cdot h_{j+1}}{1 + \varepsilon} + \frac{\alpha}{2} \cdot \left(\kappa_{j+\frac{1}{2}} - 1\right) \cdot \frac{1 + \varepsilon}{\varepsilon} \cdot \frac{C_j - \varepsilon \cdot C_{j+1}}{C_j - C_{j+1}} \cdot C^2_{j+\frac{1}{2}}. \qquad (23)$$

Equation (23) may be applied only in the case $C_j - C_{j+1} \neq 0$. Otherwise, i.e. when $C_j - C_{j+1} = 0$, the unsteadiness from the equation (23) is to be treated accordingly [**4**].

With help of equation (23) one can now also determine Roe's averaged value of the local speed of sound

$$a^2_{j+\frac{1}{2}} = \left(\kappa_{j+\frac{1}{2}} - 1\right) \cdot \left(h_{j+\frac{1}{2}} - \frac{\alpha}{2} \cdot C^2_{j+\frac{1}{2}}\right). \qquad (24)$$

The fourth scalar equation of (21) provides Roe's averaged value of the volume fraction of a gas component

$$r_{i\,j+\frac{1}{2}} = \frac{r_{i\,j} + \varepsilon \cdot r_{i\,j+1}}{1 + \varepsilon}. \qquad (25)$$

A procedure to compute $\kappa_{j+\frac{1}{2}}$ can be found in reference [**4**].

PRESENTATION OF THE SIMULATION RESULTS AND THEIR COMPARISON WITH THE MEASUREMENTS

For validating of the simulation results an AVL 520 one-cylinder research engine of the laboratory for Power Engineering, Piston and Turbo Machines of the University of Applied Sciences Hamburg was used.

The quasi-3D method introduced above is now applied to the simulation of the gas exchange processes. The simulation results and the pressure measurements are presented here only for the flow in the intake pipe. The arrangement of all measuring points is represented in the Figure 1.

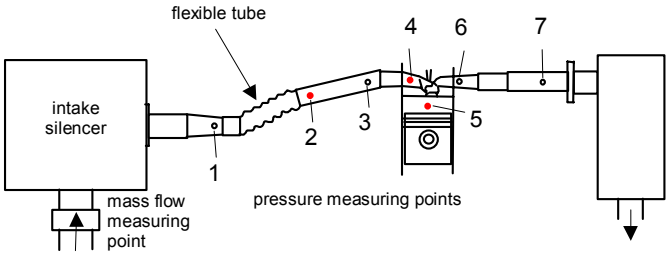

Figure 1: Arrangement of all measuring points

Figure 2 (top) shows the 3D computing mesh of the intake pipe and intake port segment, i.e., between the flexible join tube and the inlet valve, where some typical cross-sections and pressure measuring points are marking.

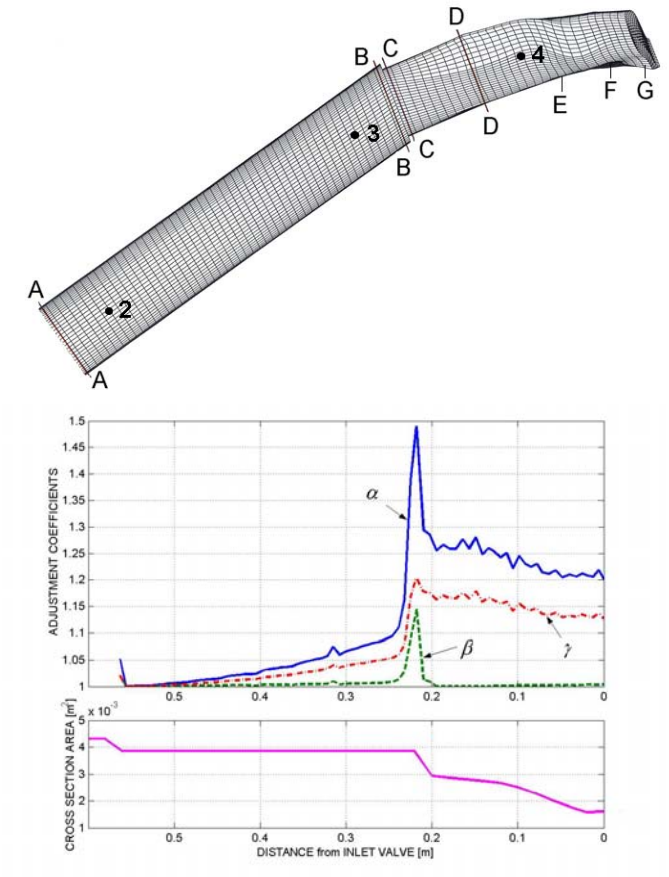

Figure 2: Intake pipe, intake pipe segment and inlet port mesh with typical cross-sections and pressure measuring points (top) and the appropriate adjustment coefficients variations (bottom)

For computing of the adjustment coefficients α, β and γ variations from Figure 2 (bottom) the 3D-flow simulation programs STAR CD and FIRE are used. This simulations are accomplished only for a compressible turbulent stady forward and reverse airflow through the intake pipe and inlet port. The flow speed vectors and isolines in the some cross-sections mentioned above are represented in Figure 3.

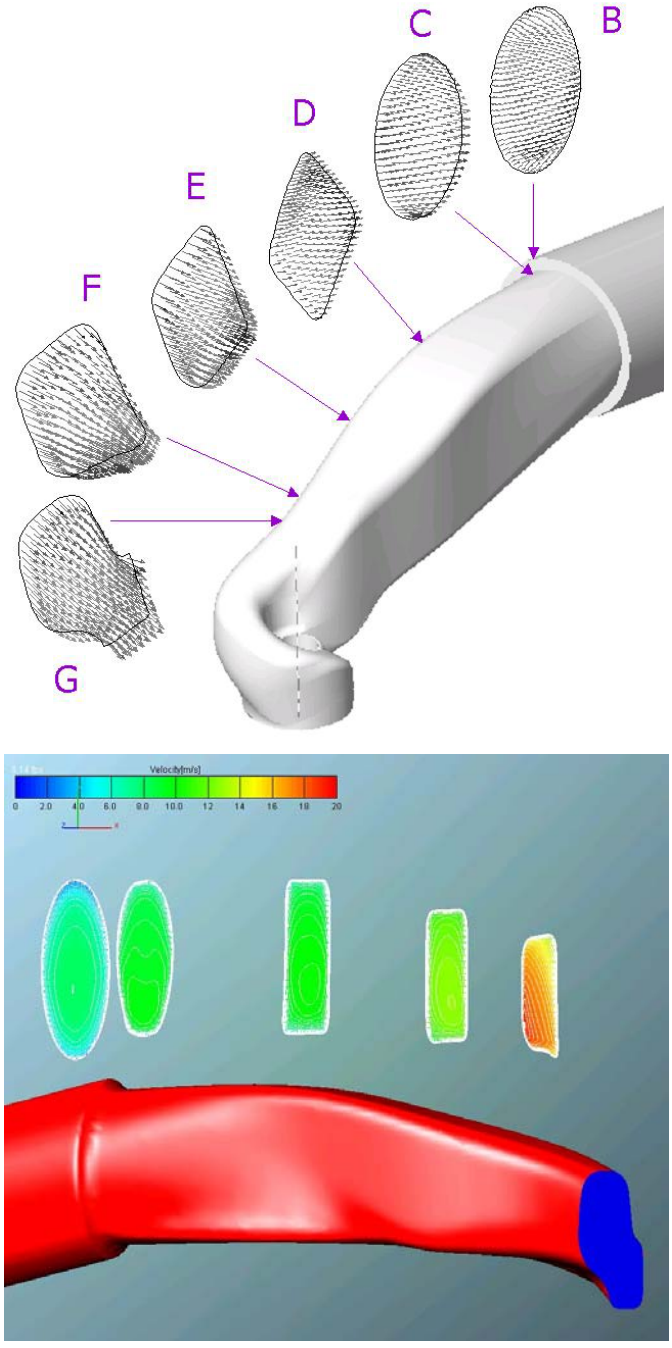

Figure 3: Flow speed vectors and isolines in some cross sections shown in the Figure 2

The analysis of all pressure variations at the measuring points shows good agreement between simulations and experiments. Some minor differences occur in any engine operating points (EOP) because:

a. only the intake pipe segment from Figures 2 and 3, i.e. between the flexible joint tube and inlet valve, is simu-

lated with the quasi-3D method and the remainder with the 1D method,

b. no other local loss coefficients for the entire intake pipe (quasi-3D segment and 1D remainder) are used in this case. Note that this combination is chosen here for easier comparison of the simulation methods (for that reason the differences between quasi-3D and 1D simulation results originate only from the influence of the adjustment coefficients from Figure 2), and

c. the supplementary (disregarded in model) wall friction and flow distortion due to the flexible joint tube between the measuring points 1 and 2 (s. Figures 1 and 4).

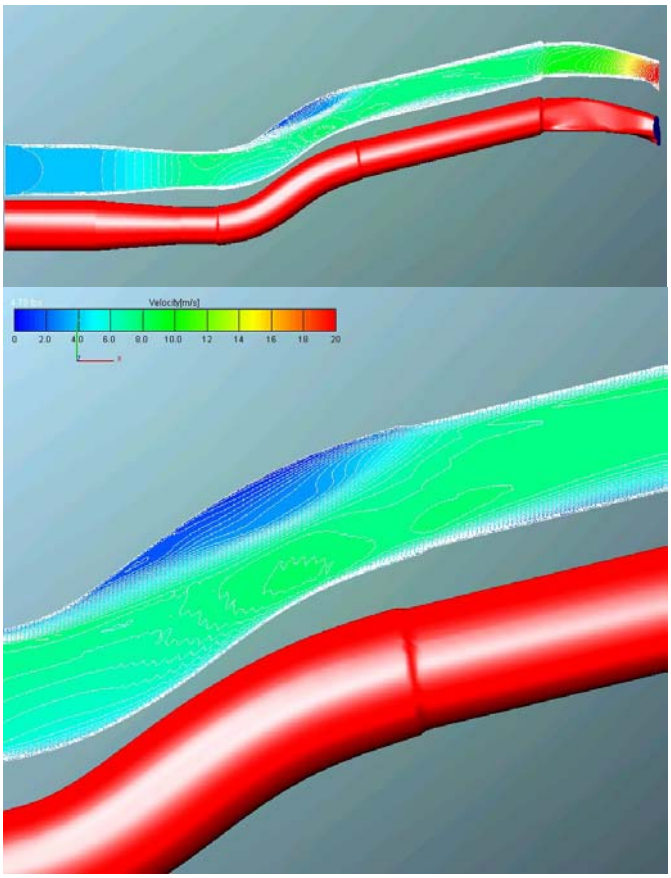

Figure 4: Intake pipe speed isolines and geometry

Two comparisons between 1D (with adjustment coefficients $\alpha, \beta, \gamma = 1$) and quasi-3D (with the adjustment coefficients from Figure 2) simulation methods are made here by EOP 46 (engine speed 2500 rpm and low load, Figure 5) and 51 (engine speed 2500 rpm and full load, Figure 6).

The comparison shows that the quasi-3D model works better and closer to the experiments and that without any adapted local loss coefficients. Although the improvement seems to be small, one must note here (because of the simplicity of the intake pipe geometry) that even the 1D method works in this case quite well. On the other hand only a segment of this pipe is treated here with the quasi-3D method as mentioned.

One expects that the differences between quasi-3D and 1D simulations will be more significant in case of complicated pipe geometry, pipe junctions and manifolds.

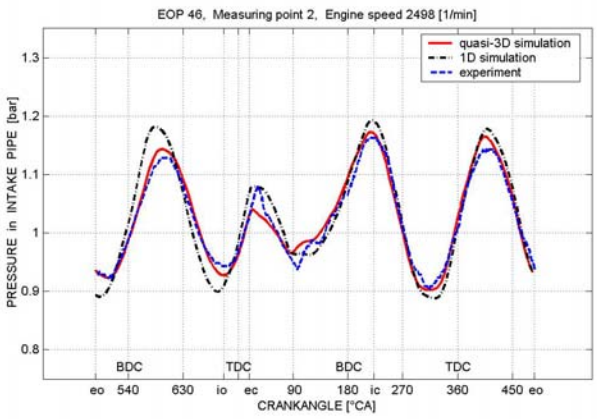

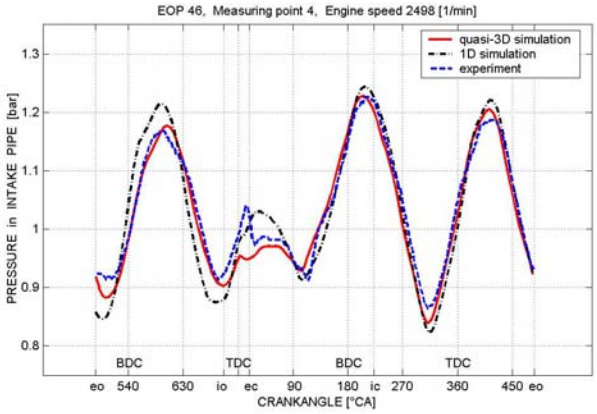

Figure 5: Comparisons between quasi-3D and 1D simulation methods by EOP 46 at measuring points 2 and 4

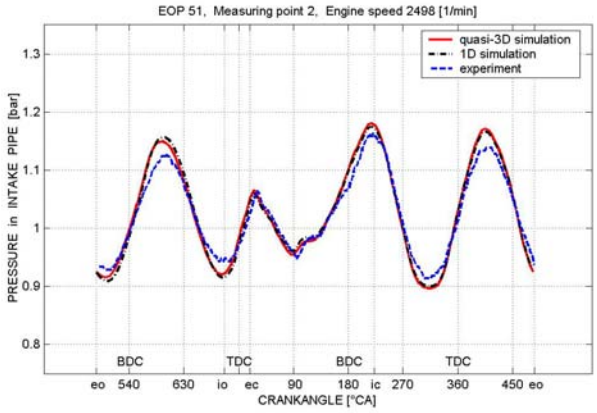

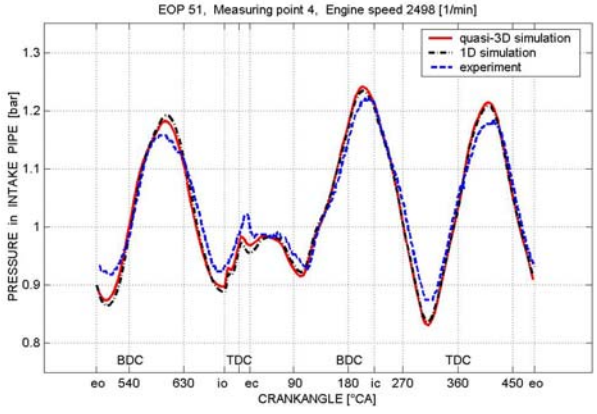

Figure 6: Comparisons between quasi-3D and 1D simulation methods by EOP 51 at measuring points 2 and 4

The quasi-3D method allows one to take into consideration the real distribution of losses along the pipes (as curvatures, asymmetry of the pipes and channels etc). On the contrary the 1D method requires artificial concentration of the distributed losses in some cross sections, which are treated during the simulation as discontinuity interfaces or boundaries [**11**]. On one hand, the treatment of the boundaries is very time-consuming and causes convergence problems frequently. On the other hand the simulation results are inaccurate close to the boundaries. This fact becomes more critical because of the complexity of modern manifolds, which requires inserting a series of boundaries along a pipe.

CONCLUSION

The quasi-3D method is introduced here as a compromise between the 1D and true-3D methods. This new method improves the quality of the 1D-simulation results noticeably, without increasing the cost of computation proportionally.

For even better accuracy, it is recommended to compute the adjustment coefficients for some forward and reverse flow rates through all the pipes if for example transition laminar-turbulent flow could appear.

One must conclude that for the treatment of multi-pipe junctions with the quasi-3D method an appropriate procedure is needed. The adjustment coefficients must be computed in this case for all flow possibilities (flow direction and some flow rates) through these multi-pipe junctions, i.e., the steady true-3D simulation must be carried out several times. This expense remains still low because in this steady simulation only the exit boundary conditions are changed and the computing time makes almost no difference in this case. The accuracy gain of the quasi-3D method will be important because of the use of appropriate adjustment coefficients, which take into consideration the refined real geometry of these multi-pipe junctions.

REFERENCES

1. Benson, R. S., Garg, R.D., and Woollatt, D., *A numerical solution of unsteady flows problems*, Int. J. Mech. Sci., 6, 117-144, 1964
2. Boussinesq, I., *Memoire sur l´influence des frottments dans les mouvements réguliers des fluides*, J. de math. pur et appl., nr. 13, p. 377, (French) 1868
3. Florea, J., Panaitescu, V., *Mecanica fluidelor*, EDP- Bucuresti (Romanian), 1979
4. Gheorghiu, V., *Higher Accuracy through Combining of quasi-3D (instead of 1D) with true-3D Manifold Flow Models during the Simulation of ICE Gas Exchange Processes,* SAE Paper 2001-01-1913, Orlando, 2001
5. Idelchik, I. E., *Handbook of hydraulic-resistance*, Springer Verlag, 1986
6. Jenny, E., *One-dimensional transient flow with consideration of friction, heat transfer and charge of section*, Brown Boveri Rev. 37, 447-461, 1950
7. Riemann, B., *Über die Fortpflanzung ebener Luftwellen von endlicher Schwingungsweite*, Gott. Abh. 8 (Math.) 43-65 (German), 1858/59
8. Roe, P. L., *Approximate Riemann solvers, parameter vectors and difference schemes*, J. Comp. Phys., Vol. 43. 357-372, 1981
9. Schillmueller, J., *Experimental investigation of the gas exchange processes at a AVL one-cylinder research engine*, Graduate paper at the University of Applied Sciences Hamburg (German), 1997
10. Seifert, H., *Instationäre Strömungsvorgänge in Rohrleitungen an Verbrennungskraftmaschinen*, Springer Verlag (German), 1962
11. Winterbone, D. E., Pearson, R. J., *Design techniques for engine manifolds - Wave action methods for IC engines*, Professional Engineering Publishing, 1999
12. Yee, H.-C., *A class of high resolution explicit and implicit shock capturing methods*, Karman Institutes for Fluid Dynamics, Lecture Series 1989-04
13. Zierep, J., *Grundzüge der Strömungslehre*, Springer Verlag (German), 1997